APPENDIX E

NTRD DOCUMENT COVER SHEET[1]

Name/Title of Deliverable/Milestone/Revision No.	Evaluation of Gas and Particle Transport through Stress Corrosion Cracks (M3SF-18SN010201047)
Work Package Title and Number	Stress Corrosion Cracking and Dry Storage Investigations – SNL (SF-18SN01020104)
Work Package WBS Number	1.08.01.02.01
Responsible Work Package Manager	Charles Bryan (Name/Signature)
Date Submitted	

Quality Rigor Level for Deliverable/Milestone[2]	☐ QRL-1 ☐ Nuclear Data	☐ QRL-2	☐ QRL-3	☒ QRL-4 Lab QA Program[3]

This deliverable was prepared in accordance with Sandia National Laboratories
(Participant/National Laboratory Name)

QA program which meets the requirements of

☒ DOE Order 414.1 ☐ NQA-1 ☐ Other

This Deliverable was subjected to:

☒ Technical Review ☐ Peer Review

Technical Review (TR)
Review Documentation Provided

☐ Signed TR Report or,
☐ Signed TR Concurrence Sheet or,
☒ Signature of TR Reviewer(s) below

Peer Review (PR)
Review Documentation Provided

☐ Signed PR Report or,
☐ Signed PR Concurrence Sheet or,
☐ Signature of PR Reviewer(s) below

Name and Signature of Reviewers

Charles Morrow

NOTE 1: *Appendix E should be filled out and submitted with the deliverable. Or, if the PICS:NE system permits, completely enter all applicable information in the PICS:NE Deliverable Form. The requirement is to ensure that all applicable information is entered either in the PICS:NE system or by using the NTRD Document Cover Sheet.*

- *In some cases there may be a milestone where an item is being fabricated, maintenance is being performed on a facility, or a document is being issued through a formal document control process where it specifically calls out a formal review of the document. In these cases, documentation (e.g., inspection report, maintenance request, work planning package documentation or the documented review of the issued document through the document control process) of the completion of the activity, along with the Document Cover Sheet, is sufficient to demonstrate achieving the milestone.*

NOTE 2: *If QRL 1, 2, or 3 is not assigned, then the QRL 4 box must be checked, and the work is understood to be performed using laboratory QA requirements. This includes any deliverable developed in conformance with the respective National Laboratory / Participant, DOE or NNSA-approved QA Program.*

NOTE 3: *If the lab has an NQA-1 program and the work to be conducted requires an NQA-1 program, then the QRL-1 box must be checked in the work Package and on the Appendix E cover sheet and the work must be performed in accordance with the Lab's NQA-1 program. The QRL-4 box should not be checked.*

Measurement of Particulate Retention in Microchannel Flows

Spent Fuel and Waste Disposition

Prepared for
US Department of Energy
Spent Fuel and Waste Science and Technology

S.G. Durbin
E.R. Lindgren
R.J.M. Pulido

Sandia National Laboratories
September 19, 2018
Milestone No. M3SF-18SN010201047
SAND2018-10522 R

Prepared by
Sandia National Laboratories
Albuquerque, New Mexico 87185 and Livermore, California 94550

Sandia National Laboratories is a multimission laboratory managed and operated by National Technology and Engineering Solutions of Sandia, LLC, a wholly owned subsidiary of Honeywell International, Inc., for the U.S. Department of Energy's National Nuclear Security Administration under contract DE-NA0003525.

ABSTRACT

The purpose of this study was to explore the flow rates and aerosol retention of an engineered microchannel with characteristic dimensions similar to those of stress corrosion cracks (SCCs) that could form in dry cask storage systems (DCSS) for spent nuclear fuel. Additionally, pressure differentials covering the upper limit of commercially available DCSS were studied. Given the scope and resources available, these data sets should be considered preliminary and are intended to demonstrate a new capability to characterize SCC under well-controlled boundary conditions.

The gap of the microchannel tested was 28.9 μm (0.00110 in.), the width was 12.7 mm (0.500 in.), and the length was 8.86 mm (0.349 in.). Over a nine-hour period, the average mass concentration upstream of the microchannel was 0.048 mg/m^3 while the average concentration downstream was 0.030 mg/m^3. By the end of the test, the mass of aerosols that entered the test section upstream of the microchannel was 0.207 mg and the mass of aerosols that exited the microchannel was 0.117 mg. Therefore, 44% of the aerosols available for transmission was retained upstream of microchannel.

This page is intentionally left blank.

ACKNOWLEDGEMENTS

The authors would like to gratefully acknowledge the hard work and commitment to excellence of Gabriel Lucero, Andres Sanchez, Shannon Zubersky, William Chavez, and Greg Koenig, which made the success of this project possible.

This work was conducted under the Department of Energy Spent Fuel and Waste Science and Technology campaign. Sylvia Saltzstein (8845) and Geoff Freeze (8843) are to be commended for exceptional project leadership.

This page is intentionally left blank.

CONTENTS

This page is intentionally left blank.

LIST OF FIGURES

LIST OF TABLES

ACRONYMS

AED	aerodynamic equivalent diameter
APS	aerosol particle sizer
DCSS	dry cask storage systems
DOE	US Department of Energy
DPC	dual-purpose canister
EDM	electrical discharge machining
FCRD	Fuel Cycle Research and Development
FY	fiscal year
PSL	polystyrene latex
PWR	pressurized water reactor
SCC	stress corrosion crack
SFWD	Spent Fuel and Waste Disposition
slpm	standard liter per minute
SNF	spent nuclear fuel
SNL	Sandia National Laboratories

This page is intentionally left blank.

MEASUREMENT OF PARTICULATE RETENTION IN MICROCHANNEL FLOWS

This report fulfills milestone M3SF-18SN010201047 in the Stress Corrosion Cracking and Dry Storage Investigations work package (SF-18SN01020104). This work was sponsored under the Department of Energy's (DOE) Office of Nuclear Energy (NE) Spent Fuel and Waste Disposition (SFWD) campaign.

1 INTRODUCTION

Dry cask storage systems (DCSS) for spent nuclear fuel (SNF) are designed to provide a confinement barrier that prevents the release of radioactive material, maintain SNF in an inert environment, provide radiation shielding, and maintain subcriticality conditions. SNF is initially stored in pools of water for cooling where the water also provides radiation shielding. As these pools get closer to capacity, dry storage systems are becoming the primary alternative for interim storage. After sufficient cooling in pools, SNF is loaded into a canister and placed inside a storage cask, where the canister is welded shut. Then the dry storage cask system is decontaminated and dried, and the system is ultimately sent to a storage location. Figure 1 shows the major components of a dry storage cask for spent nuclear fuel.

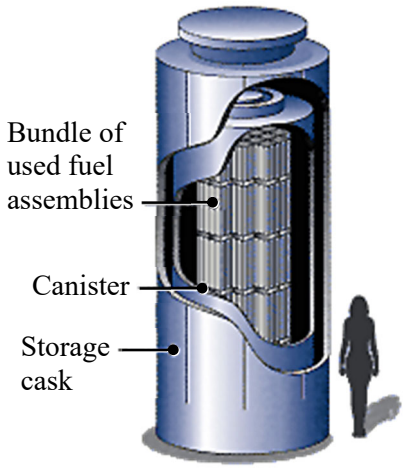

Source: https://www.nrc.gov/waste/spent-fuel-storage/diagram-typical-dry-cask-system.html

Figure 1. Typical dry storage cask.

Typically, the canisters are made of stainless steel. The open volume between the canister and the cask allows passive ventilation from outside air, which can impart dust that collects on the surfaces of the canister. As the SNF cools, salts contained in the dust may deliquesce to form concentrated brines, which may contain corrosive species such as chlorides. These species are capable of causing localized corrosion, called pitting. With sufficient stresses, these pits can evolve into stress corrosion cracks (SCCs), which could penetrate through the canister wall and allow communication from the interior of the canister to the external environment [Schindelholz, 2017].

1.1 Objective

The purpose of this study was to explore the flow rates and aerosol retention of an engineered slot with characteristic dimensions similar to those in SCCs. Additionally, pressure differentials covering the upper limit of commercially available dry cask storage systems (DCSS) were studied. Given the scope and resources available, these data sets should be considered preliminary and are intended to demonstrate a new capability to characterize SCC under well-controlled boundary conditions.

1.2 Previous Studies

The data obtainable from the measurement of particulate segregation in flows through open channels has significance in multiple fields. Studies include particle penetration through building cracks [Lewis, 1995, Liu and Nazaroff, 2003, Mosley *et al.*, 2001] to nuclear reactor safety [Powers, 2009], and more recently, storage and transportation of spent nuclear fuel in dry casks. Study of these systems contribute to the understanding of particulate segregation through small channels as functions of particle size, channel dimensions, and differential pressures.

Previous work has contributed to the characterization of particulate segregation across channel flow for a range of particle sizes in aerosols. Lewis [Lewis, 1995] was motivated by a lack of empirical studies to support the development of protection factors against solid particles for enclosures. This protection factor was taken as the ratio of the dose of an outside concentration of particulates to the dose accumulated inside an enclosure for a specified time, with the doses defined as concentration-time integrals. Models were derived describing the total transport fraction of particles across a rectangular slot into an enclosure as functions of particle size, differential pressures, and slot heights. Lewis described an experimental apparatus with synthesized aerosols (containing either talc, aluminum oxide, titanium oxide, various silica powders, or ambient dust) mixed in a chamber containing an enclosure with a rectangular slot open to the chamber. A differential pressure was established between the chamber and the enclosure. Protection factors were found by comparing mass concentration values inside and outside the enclosure over a given time. The primary observations here were the decrease in total transport fraction with increasing particle size from 1-10 μm as well as a decrease in protection factor (corresponding to an increase in total transport fraction) with increasing differential pressures and slot heights.

Liu and Nazaroff [Liu and Nazaroff, 2003] conducted experiments of aerosol flow through rectangular slots using various building materials, including aluminum, brick, concrete, and wood. The slot heights were 0.25 mm and 1 mm, which are large compared to the micron- to submicron-sized particles they flowed through the cracks. They obtained data for particle penetration (defined as the ratio of downstream to upstream particle concentration), related to total transport fraction, as a function of particle size and found that, for 0.25 mm cracks, particle sizes between 0.1-1 μm achieved penetration factors near unity, while smaller and larger particles showed diminished penetration factors for pressure differentials of 4 and 10 Pa. Meanwhile, for 1 mm slot heights, the penetration factors were near unity for the majority of the particle size distribution. Their results matched closely with models they created from analysis of particle penetration through simplified cracks [Liu and Nazaroff, 2001] and had similar qualitative conclusions to Lewis's work.

Mosley *et al.* [Mosley *et al.*, 2001] studied particle penetration through a 0.508 mm slot height between aluminum plates with particles of aerodynamic equivalent diameters (AED) from 0.1 to 5 μm. They found penetration factors close to unity for particle sizes between 0.1-1 μm, with a sharp drop-off in penetration factor for particle sizes larger than 1 μm for pressure differentials between 2 and 20 Pa – this was consistent with Liu and Nazaroff's results when considering the order of magnitude of the pressure differentials and particle size distributions.

1.3 Uniqueness of Current Study

The motivation behind the aforementioned work was based on ambient particle penetration of enclosures and the amount of particles subject to human exposure, with slot heights and pressure differentials corresponding to conditions typically associated with building cracks and pressure differences between indoor and outdoor environments, respectively. However, the channel dimensions considered do not apply to the channel geometry associated with cracks from potential corrosion of dry casks. The literature reports typical crack heights to be around 16 to 30 μm [EPRI, 2017, EPRI, 2014, Meyer, 2013] and internal pressures of 100 to 760 kPa (14.5 to 110 psig) [EPRI, 2017] for a range of cask models. Therefore, an apparatus and procedures were developed to investigate a slot height on the order of tens of

microns and pressure differentials on the order of hundreds of kPa to supplement the established database of particulate retention in microchannel flows. This experimental approach is intended to be adaptable for future testing of more prototypic stress corrosion crack geometries.

This page is intentionally left blank.

2 APPARATUS AND PROCEDURES

The experimental approach adopted for these studies is similar to previous studies [Lewis, 1995; Mosley *et al.*, 2001; and, Liu and Nazaroff, 2001 and 2003] in that aerosol analyzers are used to characterize the particle size distribution and concentration present in the gas before and after flowing through a simulated crack. Because these previous studies considered aerosol transport through building walls or containment structures, the focus was on flows through relatively wide and long slots driven by constant low pressure drops. In the present study, consideration is given to aerosol transport through dry storage canister walls. Here, the focus is on much narrower and shorter microchannels that represent stress corrosion cracks through the canister wall driven by initially higher pressure drops. Furthermore, the pressure drop is not constant but transient to simulate the blowdown from canister depressurization.

2.1 General Construction

The general layout of the experimental setup is illustrated in Figure 2 and Figure 3. A 0.908 m^3 (240 gal) pressure tank is used to simulate the canister. The tank was pressurized and loaded with a measured amount of aerosols. Flow from the tank into the test section was measured by a mass flow meter. The engineered microchannel, simulating a crack, was mounted in the middle of the test section. A sample stream was metered from the high-pressure upstream and low-pressure downstream side of the simulated crack for aerosol size and concentration characterization using identical TSI Model 3321 Aerodynamic Particle Sizer (APS) Spectrometers. The pressure of the upstream sample was reduced to ambient by a mass flow controller that metered the flow to the upstream APS. An open-to-ambient, overflow line was used to protect the upstream APS from over-pressurization in the event of a control valve failure. A mass flow meter measured the sample flow drawn into the downstream APS. Pressure was monitored on the upstream and downstream sides of the microchannel using pressure transducers. A low pressure drop HEPA filter was used to remove all aerosols from the exhaust stream.

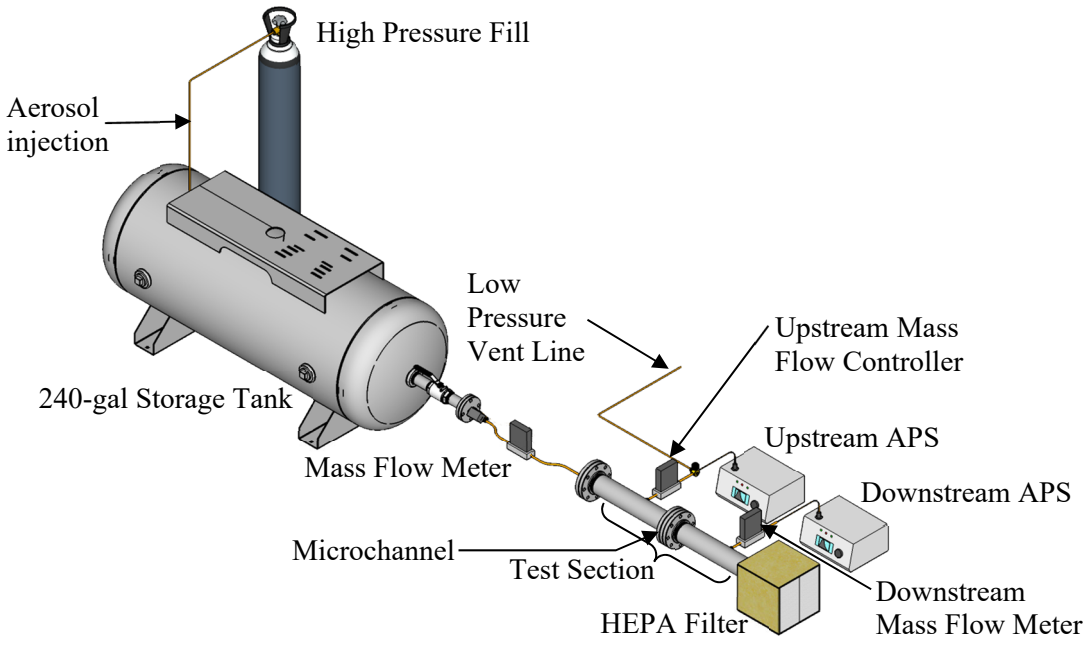

Figure 2. General layout of the experimental apparatus.

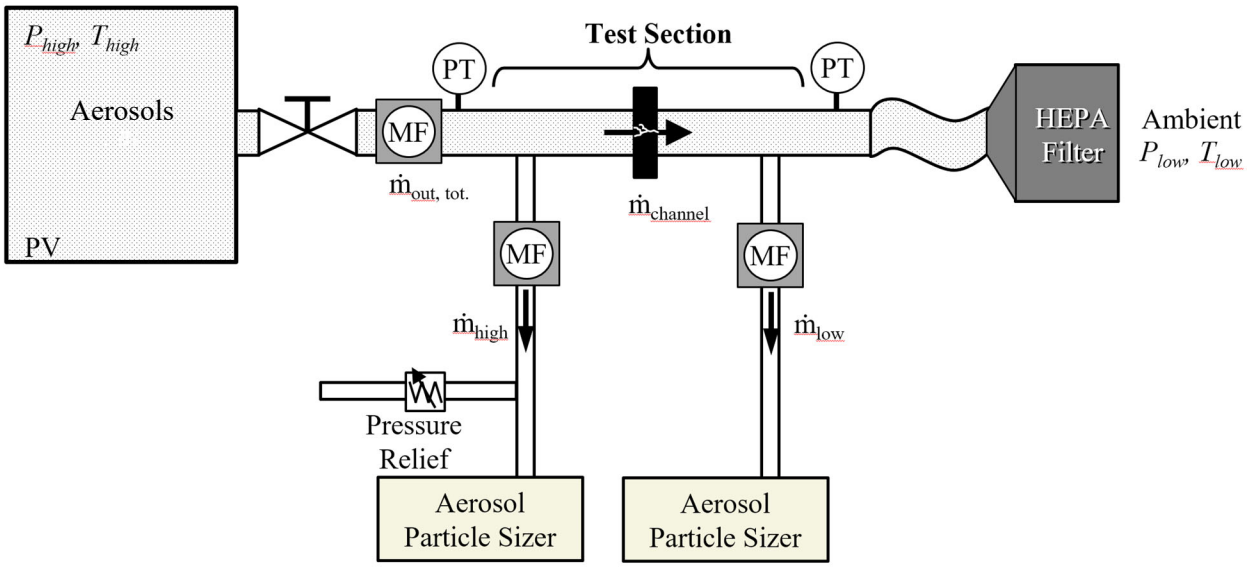

Figure 3. Schematic of the apparatus showing the major components.

2.2 Design of the Microchannel

The engineered microchannel was fabricated from paired high-precision Mitutoyo gage blocks. The microchannel was machined into the surface of one gage block using electrical discharge machining (EDM). The mounting holes were also cut using wire EDM. As shown in Figure 4 the dimensions of the microchannel are 12.7 mm (0.500 in.) wide, 8.86 mm (0.349 in.) long and an average of 28.9 μm (0.0011 in.) deep. The paired halves of the gage blocks are bolted together to form the microchannel held in a mounting assembly as detailed in Figure 5. An isometric view of the microchannel mounted to the flow flange is shown in Figure 6.

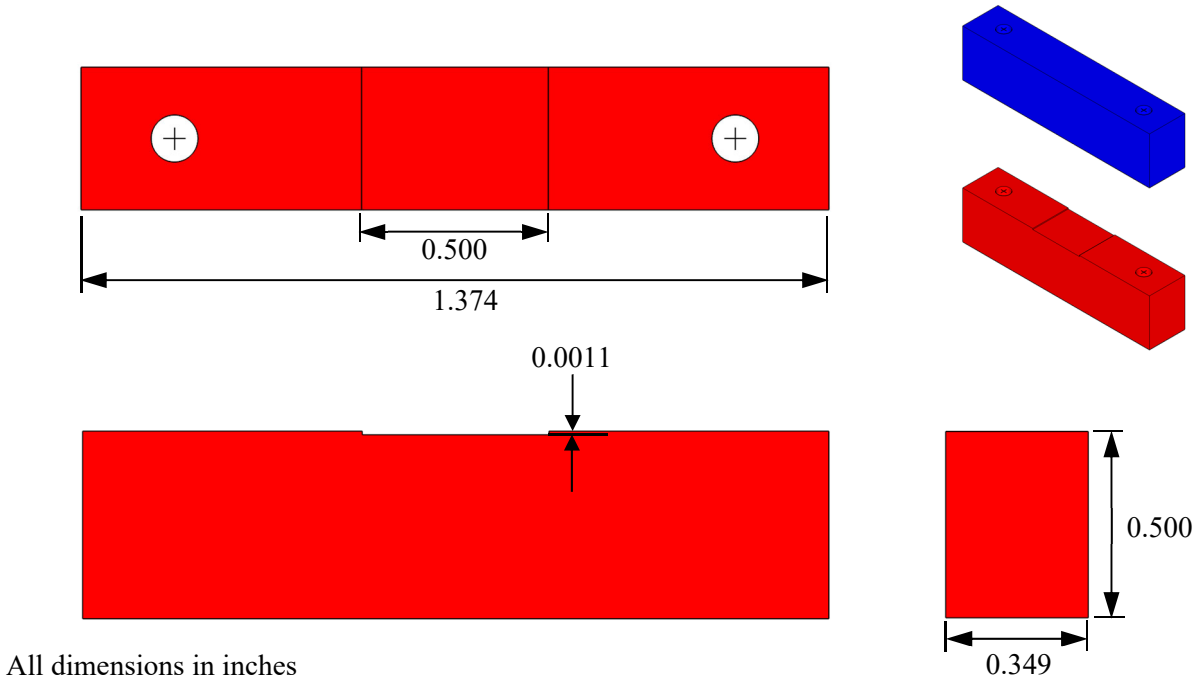

Figure 4. Schematic of the microchannel assembly.

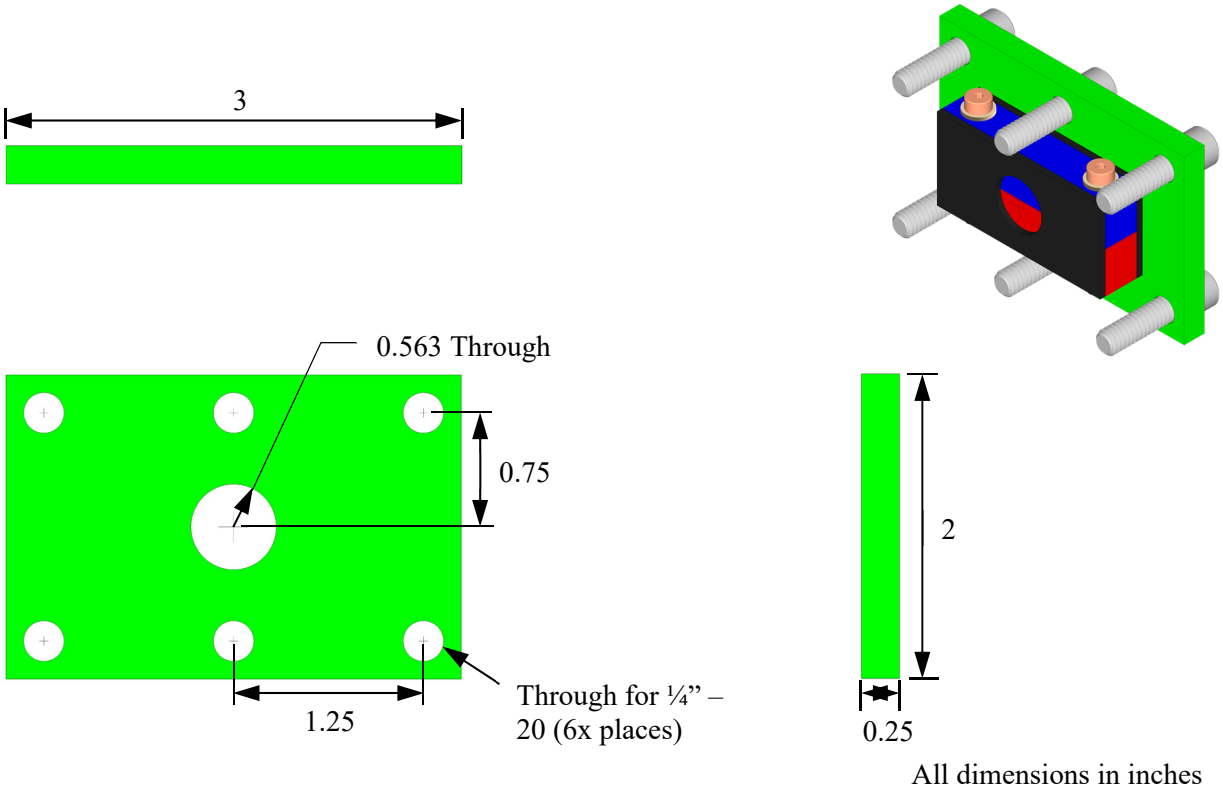

Figure 5. Details of the microchannel mounting assembly.

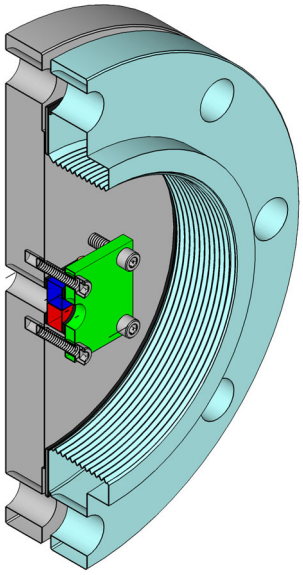

Figure 6. Isometric cutaway showing the microchannel mounted to the flow flange.

Figure 7 shows profilometry of the microchannel on both sides of the as-built microchannel. These scans represent approximately 1.2 mm (0.047 in.) of the overall 12.7 mm (0.500 in.) slot, or 9%. The average step height based on these measurements is 28.9 µm (0.0011 in.). These profiles were taken with a Keyence VK-X100 laser scanning microscope.

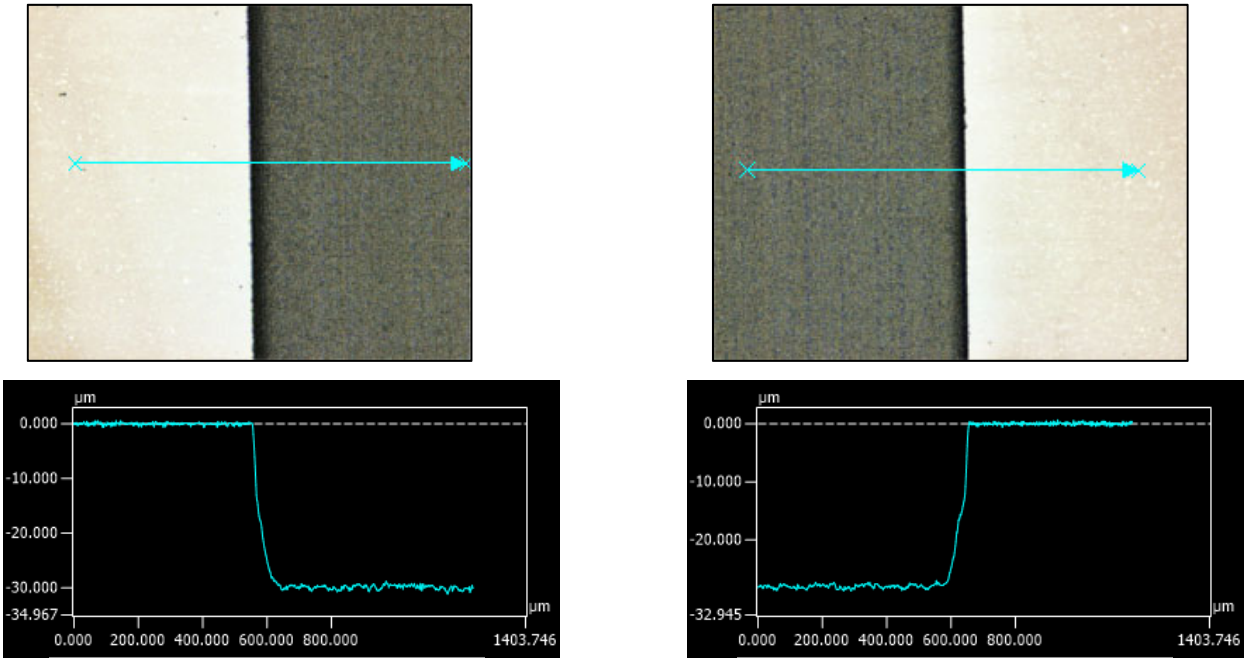

Area average step height 29.9 µm

Area average step height 27.9 µm

Figure 7. Profilometry of the microchannel orifice.

During the profilometry the surface roughness of the microchannel was also characterized with the Keyence VK-X100 laser scanning microscope. The results of the surface roughness characterization are given in Figure 8. In the embedded tables, S_a is the arithmetical mean height of the shown areas and is defined as the average of the difference between each surface point measurement and the mean plane of the surface. The root mean square height, S_q, is equivalent to the standard deviation of heights. Area2 is the microchannel surface and Area1 is the adjoining gage surface. By all measures the surface roughness of the microchannel was roughly twice that of the gage block surface.

Left Side 10×

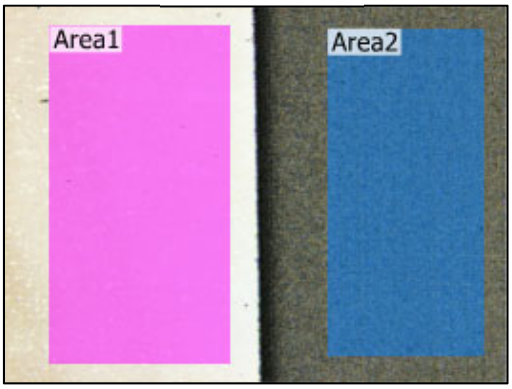

	S_a (µm)	S_q (µm)
Area1	0.213	0.275
Area2	0.408	0.520

Right Side 10×

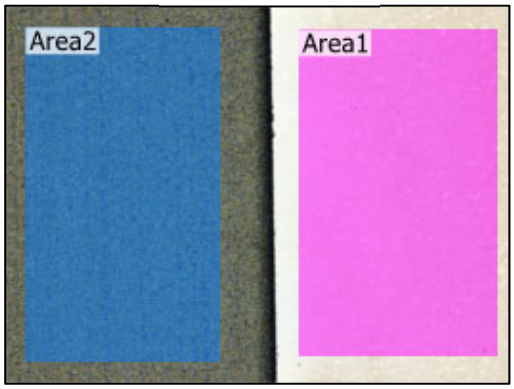

	S_a (µm)	S_q (µm)
Area1	0.238	0.300
Area2	0.386	0.494

Figure 8. Surface roughness characterizations.

2.3 Instrumentation

The following instrumentation was used to characterize these tests. All stated uncertainties are assumed to represent 95% confidence intervals unless otherwise stated.

2.3.1 Pressure

Pressure was monitored on the upstream side using a 1034 kPa (150.0 psia) Setra Model ASM transducer and on the downstream side with a 103 kPa (15.0 psia) Model ASM transducer. The pressure in the tank was monitored with a 2068 kPa (300 psia) Setra Model ASM transducer.

The accuracy of the Setra Model ASM transducers was <±0.05% full scale (FS).

Table 1. Summary of pressure transducers.

Location	Model No.	Range (kPa)	Uncertainty (kPa)
Storage tank	ASM1-300P-A-1M-2C-03-A-01	0 – 2068	1.03
Upstream	ASM1-150P-A-1M-2C-03-A-01	0 – 1034	0.52
Downstream	ASM1-015P-A-1M-2C-03-A-01	0 – 103	0.05

2.3.2 Temperature

All temperature measurements were taken with K-Type thermocouples. The suggested, combined uncertainty in these measurements including data acquisition, cabling, and positioning errors is 1% of the reading in Kelvin.

2.3.3 Gas Mass Flow Rate

Flow from the tank into the test section was measured by a mass flow meter (OMEGA Model FMA-1609A, 0 to 50 slpm). The standard liter per minute (slpm) was is defined as one liter of air flow at standard conditions of 101.325 kPa and 25 °C (*i.e.* reference density of 1.184 kg/m^3). The pressure of the upstream sample was reduced to ambient by a mass flow controller (OMEGA Model FMA-2606A-TOT, 0 to 5 slpm) that metered the flow to the upstream APS. A mass flow meter measured the sample flow drawn into the downstream APS (OMEGA Model FMA-1605A, 0 to 2 slpm).

For the FMA-1600 and FMA-2600, the reported accuracy is ± (0.8% of reading + 0.2% FS) for a maximum of ± 1% FS.

Table 2. Summary of mass flow instrumentation.

Description	Model No.	Range (slpm)	Range (kg/s)	Uncertainty (kg/s)
Storage tank to upstream	FMA-1609A	0 – 50	0 – 9.9×10^{-4}	0 – 1×10^{-5}
Upstream to APS	FMA-2606A-TOT	0 – 5	0 – 9.9×10^{-5}	0 – 1×10^{-6}
Downstream to APS	FMA-1605A	0 – 2	0 – 3.9×10^{-5}	0 – 4×10^{-7}

2.3.4 Aerosol Particle Sizer

A sample stream was metered from the high-pressure upstream and low-pressure downstream side of the simulated crack for aerosol size and concentration characterization using identical TSI Model 3321 Aerodynamic Particle Sizer Spectrometers (APS).

Concentration Accuracy	±10% of reading plus variation from counting statistics
Aerodynamic Size Resolution	0.02 μm at 1.0 μm, 0.03 μm at 10 μm
Minimum Particle Concentration	0.001 particle/cm^3
Maximum Recommended Particle Concentration	1,000 particles/cm^3 at 0.5 μm with <5% coincidence; 1,000 particles/cm^3 at 10.0 μm with <10% coincidence; usable data up to10,000 particles/cm^3

2.4 Selection of Initial Conditions

2.4.1 Surrogate Selection

Cerium oxide (CeO_2) was chosen as the surrogate for spent nuclear fuel ($\rho_{SNF} \approx 10$ g/cm^3) because of its relatively high density ($\rho_{CeO_2} = 7.22$ g/cm^3) and its commercial availability. Figure 9 shows the particle characteristic size distribution of the surrogate used in these tests. Here, the distribution is plotted as a function of aerodynamic equivalent diameter (AED). This surrogate was chosen because the particles

were concentrated in the respirable range (AED < 10 µm). Table 3 gives a summary of the aerosol characteristics of the surrogate.

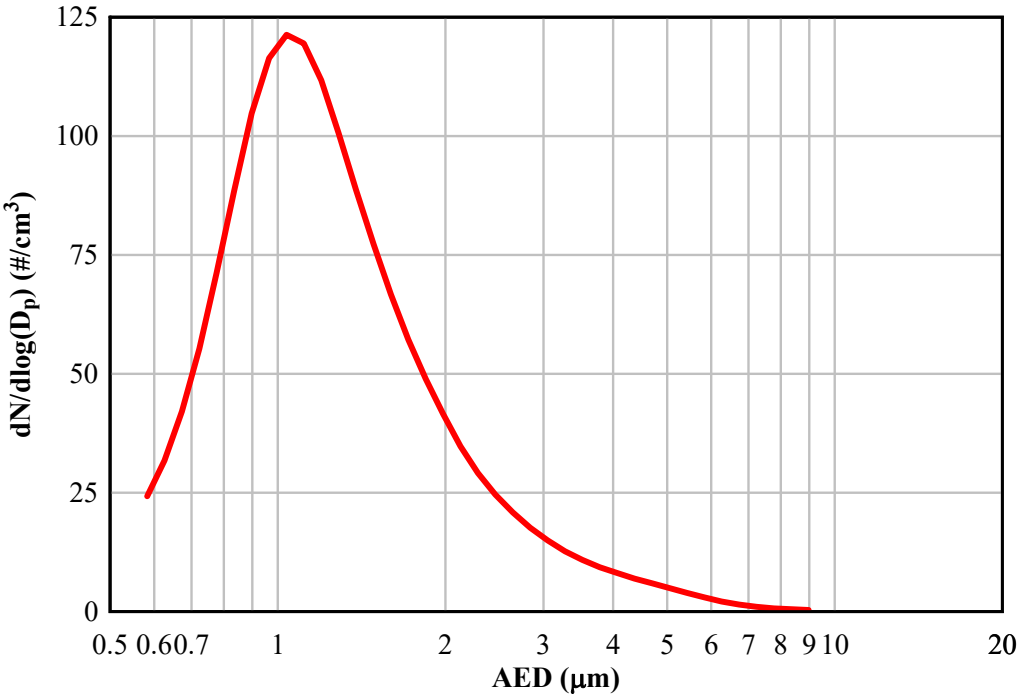

Figure 9. Particle size distribution of the cerium oxide surrogate.

Table 3. Summary of cerium oxide surrogate characteristics.

	Number Particle Size	Mass Particle Size
Median (µm)	1.18	4.12
Mean (µm)	1.36	4.81
Geometric Mean (µm)	1.24	3.98
Mode (µm)	1.07	4.22
Geometric Std. Dev.	1.47	1.88
Total Concentration	2422 (#/cm^3)	2.30 (mg/m^3)

2.4.2 Selection of Aerosol Density

An estimate of the aerosol density was needed to inform the execution of the tests. As described earlier, the tests described in this report were focused on respirable particles with an AED < 10 µm. To derive an aerosol density of interest, data from a previous study was referenced to estimate an upper bound for release of spent fuel into a canister [Hanson *et al.*, 2008]. An average release fraction across all tests was found to be 1.9×10^{-5}, where air was blown through segments of spent fuel rods and the released fuel was measured. Of this release fraction, the respirable fraction from all available data was 6.0×10^{-3}. Therefore, the respirable release fraction was estimated as the product of the two fractions to be 1.1×10^{-7}.

To estimate an upper aerosol density for spent fuel dry storage, a canister with 37 pressurized water reactor (PWR) assemblies with a mass of fuel (UO_2) 520 kg per assembly was assumed. Ten percent of the fuel was assumed to fail due to an undefined event. The fines released were assumed to recirculate within the canister without any deposition. The canister was assumed to have a starting initial pressure of 800 kPa (116 psia). The equivalent aerosol density for this assumed system at standard temperature and pressure is approximately 7 mg/m^3. For the storage tank, approximately 50 mg was needed to achieve an equivalent aerosol density. Expecting a large deposition factor, the test was started with an excess (~ 100 mg) of the respirable ceria particles aerosolized into the tank.

3 RESULTS

3.1 Line Loss Characterizations

A series of unpressurized tests with 1.0, 3.1, and 4.8 μm monodisperse polystyrene latex (PSL) beads were performed to characterize the line losses in the sample tubing and instrumentation. Here, line losses are defined as the ratio of aerosol concentration as measured through a mass flow instrument compared to the same aerosol concentration as measured without the mass flow instrument. Figure 10 shows the layout for line loss characterization. Two APS units (S868365 and S931474) were plumbed to the same sample port and a single size of PSL beads were injected into the flow path. The corresponding aerosol densities were recorded simultaneously for both APS units and compared for line losses, primarily due to the mass flow instrumentation. This procedure was repeated for each PSL size and for both the upstream and downstream sections of the test section. Note that the upstream section used a mass flow controller, and the downstream section used a mass flow meter.

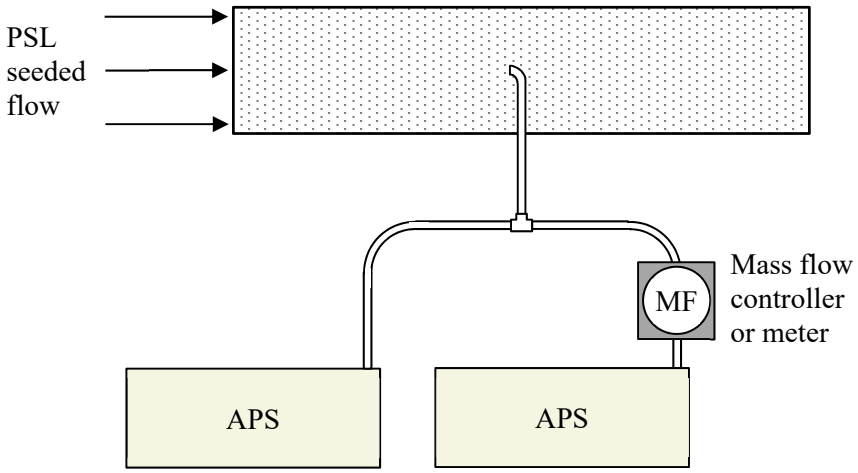

Figure 10. Schematic of line loss characterization configuration.

After examination of the PSL data, a discrepancy was detected in the outputs of the two APS units. Attempts to reconcile the difference in possible signal gain between the APS units were unsuccessful prior to testing. Therefore, an empirical correction was developed a posteriori by taking the ratio of the average, instrument-specific PSL mass concentration to the average for all PSL mass concentrations. These correction factors were determined to be 1.19 and 0.81 for S868365 and S931474, respectively. The output for each APS was corrected by dividing by the instrument-specific correction factor. Unless otherwise stated, all results presented in the remainder of this report have been corrected in this manner.

Table 4 gives the corrected mass concentrations and effective line losses for both APS units for three different PSL sizes. The overall line loss for the upstream mass flow controller was estimated to be an average of 0.47 for all particle sizes. Similarly, the overall line loss for the downstream mass flow meter was estimated to be 0.82.

These APS and line loss characterizations represent a limited number of preliminary trials. The uncertainties introduced by the instrument-specific correction factors and line loss fractions were not considered in the interpretation of the test results but are acknowledged to be significant. More attention to system characterizations is needed to better understand and reduce these uncertainties in future testing.

Table 4. Effective line losses due to mass flow instrumentation.

APS	Diameter (μm)	Upstream			Downstream		
		Controller (mg/m^3)	Open (mg/m^3)	Line Loss (-)	Meter (mg/m^3)	Open (mg/m^3)	Line Loss (-)
S868365	1.0	0.877	1.659	0.53	1.197	1.304	0.92
S931474	1.0	0.802	1.306	0.61	0.979	0.971	1.01
S868365	3.1	1.156	3.564	0.32	0.736	1.428	0.52
S931474	3.1	1.322	3.997	0.33	0.980	1.318	0.74
S868365	4.8	1.881	3.710	0.51	0.643	0.715	0.90
S931474	4.8	1.914	3.882	0.49	0.638	0.761	0.84
Average				0.47			0.82

3.2 Gas Flow Measurements

Figure 11 shows the mass flow of air through the microchannel as a function of pressure drop across the microchannel. A pre-test characterization (blue) with zero particle loading was collected using clean air and a clean microchannel. The data collected during the aerosol-laden test is shown in red. The post-test characterization (green) was conducted with zero particle loading and clean air but with the previously deposited aerosols on the microchannel left in an undisturbed state. Figure 12 shows a photo of the gage blocks making up the microchannel after the aerosol-loaded test and the post-test characterization. The microchannel is cut into the gage block in the foreground and particle deposition is evident, especially along the side walls of the microchannel. The decrease in flow rate from the pre-test characterization test to the aerosol test indicates partial plugging of the microchannel. The similarity of the aerosol test results and the post-test characterization results indicates that the microchannel particle deposition occurred early in the aerosol test.

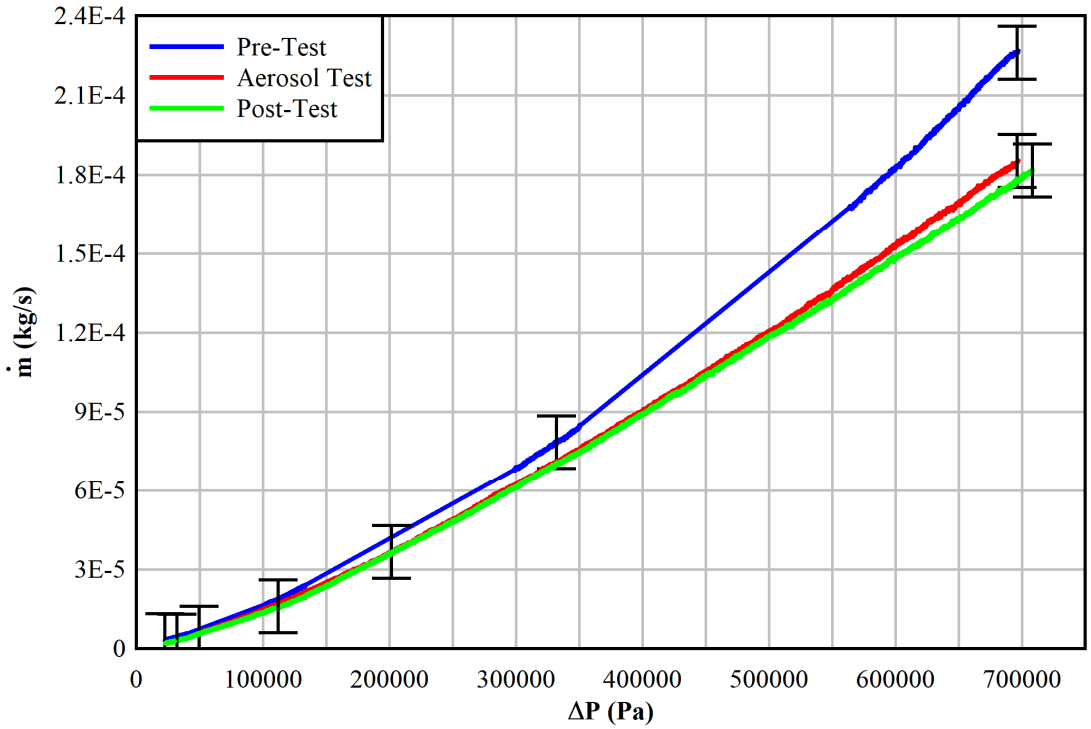

Figure 11. Mass flow rate versus pressure differential.

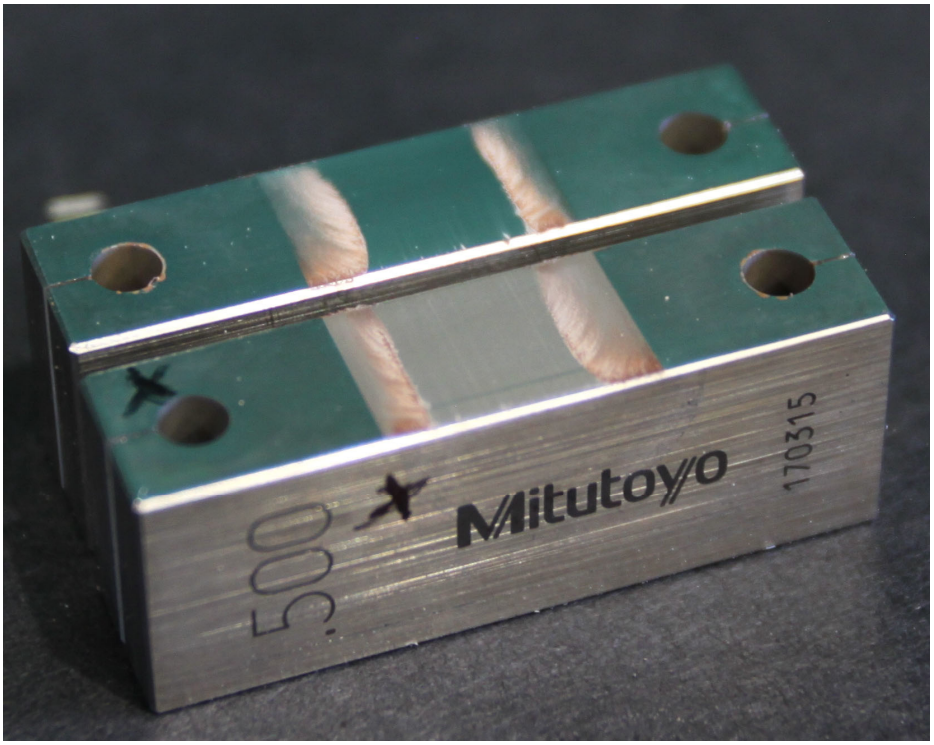

Figure 12. Photo of gage block microchannel. The microchannel is cut into the block in the foreground. Particle deposition is evident along the side walls of the microchannel.

3.3 Aerosol Measurements

Figure 13 shows the mass concentration of aerosols measured upstream and downstream of the microchannel on the left dependent axis and the air mass flow rate through the microchannel on the right dependent axis as a function of time. The mass concentration of aerosols is higher upstream of the microchannel than downstream indicating exclusion of aerosols in the flow through the microchannel. The concentration difference is greatest early in the transient when the flow through the microchannel is largest. Later, the concentrations become equivalent after approximately five hours. Over the nine-hour period, the average mass concentration upstream was 0.048 mg/m^3 while the average concentration downstream was 0.030 mg/m^3. The transient aerosol mass flow rate and integral total aerosol mass is shown in Figure 14. By the end of the test, the mass of aerosols that entered the test section upstream of the microchannel was 0.207 mg and the mass of aerosols that exited the microchannel was 0.117 mg for an overall retention of 0.44.

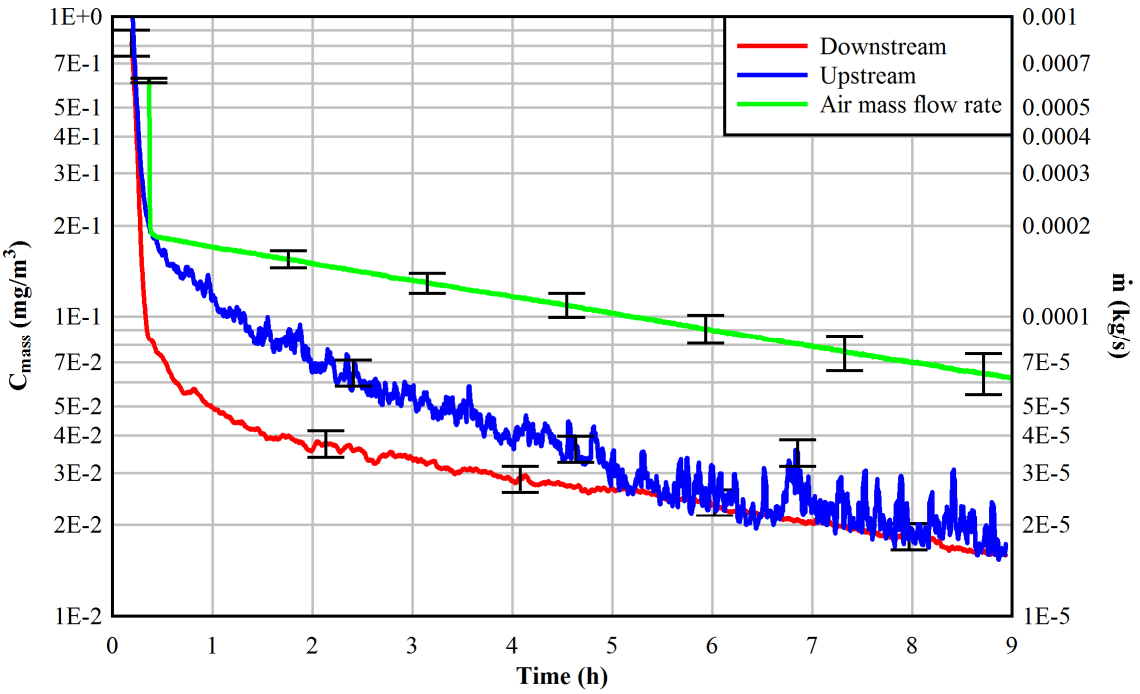

Figure 13. Air mass flow rate through the microchannel and the aerosol mass concentration for upstream and downstream sampling as a function of time.

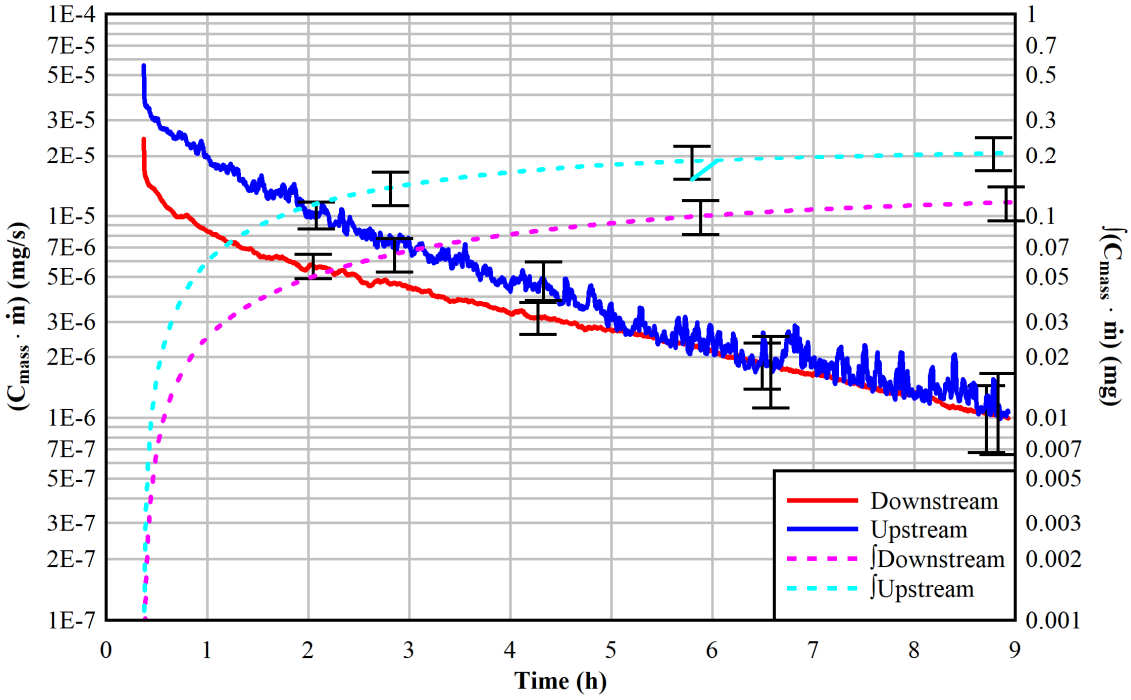

Figure 14. Transient aerosol mass flow rate and integral total aerosol mass.

This page is intentionally left blank.

4 Summary

The purpose of this study was to explore the flow rates and aerosol retention of an engineered microchannel with characteristic dimensions similar to those in stress corrosion cracks that hypothetically could form in dry storage canister walls. Additionally, pressure differentials covering the upper limit of commercially available dry cask storage systems were studied. Given the scope and resources available, these data sets should be considered preliminary and are intended to demonstrate a new capability to characterize stress corrosion cracks under well-controlled boundary conditions.

The gap of the microchannel tested was 28.9 μm (0.0011 in.), the width was 12.7 mm (0.500 in.) and the length was 8.86 mm (0.349 in.). Over a nine-hour period, the average mass concentration upstream of the microchannel was 0.048 mg/m^3 while the average concentration downstream was 0.030 mg/m^3. By the end of the test, the mass of aerosols that entered the test section upstream of the microchannel was 0.207 mg and the mass of aerosols that exited the microchannel was 0.117 mg. Therefore, 44% of the aerosols available for transmission was retained upstream of microchannel.

This page is intentionally left blank.

5 References

EPRI, "Flaw Growth and Flaw Tolerance Assessment for Dry Cask Storage Canisters," EPRI 3002002785 Electric Power Research Institute, Palo Alto, CA, October (2014).

EPRI., "Dry Cask Storage Welded Stainless Steel Canister Breach Consequence Analysis Scoping Study," EPRI 3002008192, Electric Power Research Institute, Palo Alto, CA, November (2017).

Hanson, B.D., R.C. Daniel, A.M. Casella, R.S. Wittman, W. Wu (BSC), P.J. MacFarlan, and R.W. Shimskey, "Fuel-In-Air FY07 Summary Report," PNNL-17275, Pacific Northwest National Laboratory, Richland, Washington, September (2008).

Lewis, S., "Solid Particle Penetration into Enclosures", J. Hazardous Materials, *43,* 195-216, (1995).

Liu, D-L.and W.W. Nazaroff, "Modeling Pollutant Penetration Across Building Envelopes," **Atmos. Environm**., ***35,*** 4451-4462, (2001).

Liu, D-L. and W.W. Nazaroff, "Particle Penetration Through Building Cracks," **Aerosol Science and Technology**, ***37***, 565-573, (2003).

Meyer, R. M., *et al*., "Evaluating Conventional NDE Methods for Crack Detection in Metal Canisters," Presentation at *Extended Storage Collaboration Program (ESCP)*, December 4, (2013).

Mosely, R.B., D.J. Greenwell, L.E. Sparks, Z. Guo, W.G. Tucker, R. Fortmann, C. Whitfield, "Penetration of Ambient Fine Particles into the Indoor Environment," **Aerosol Science and Technology**, ***34***, 127-136, (2001).

Powers, D.A., "Aerosol Penetration of Leak Pathways – An Examination of the Available Data and Models," SAND2009-1701, Sandia National Laboratories, Albuquerque, NM, April (2009).

Schindelholz, E., C. Bryan, and C. Alexander, "FY17 Status Report: Research on Stress Corrosion Cracking of SNF Interim Storage Canisters," SAND2017-10338R, Sandia National Laboratories, Albuquerque, NM, August (2017).